Statistical mixture design for carbide residue activated blast furnace slag foamed lightweight concrete

Zhang, Hongzhi; He, Yanchen; Wang, Chuan; Guan, Yanhua; Ge, Zhi; Sun, Renjuan; Ling, Yifeng; Šavija, Branko

DOI
10.1016/j.conbuildmat.2022.127840

Publication date
2022

Document Version
Final published version

Published in
Construction and Building Materials

Construction and Building Materials 342 (2022) 127840

Contents lists available at ScienceDirect

Construction and Building Materials

journal homepage: www.elsevier.com/locate/conbuildmat

Statistical mixture design for carbide residue activated blast furnace slag foamed lightweight concrete

Hongzhi Zhang [a,b], Yanchen He [a], Chuan Wang [c], Yanhua Guan [a], Zhi Ge [a,*], Renjuan Sun [a], Yifeng Ling [a,*], Branko Šavija [d]

[a] School of Qilu Transportation, Shandong University, 250002, Jinan, PR China
[b] Suzhou Research Institute, Shandong University, Suzhou 215021, PR China
[c] Shandong Hi-speed Group, 250098, Jian, PR China
[d] Microlab, Faculty of Civil Engineering and Geosciences, Delft University of Technology, 2628 CN, Delft, The Netherlands

ARTICLE INFO

Keywords:
Carbide residue
Blast furnace slag
Foamed lightweight concrete
Statistical mixture design

ABSTRACT

Carbide residue activated blast furnace slag is a relatively new kind of eco-friendly construction materials. This work addresses the design of foamed lightweight concrete as road embankment material using such material. A statistical mixture design approach was adopted to assess the influence of each ingredient as well as the interaction between these on the spreadability and compressive strength and thus allowing mixture design. The fitted models were validated using analysis of variance, residual analysis and confirmed by the experiments. Afterwards, the proposed models were used to optimize the mixture. The mixture with the highest compressive strength and the maximum content of carbide residue that allows the mixture to meet the required properties were obtained, respectively.

1. Introduction

Foamed concrete is a lightweight cellular construction material which has random air voids created by the entrapped foam agent. Advantages like low weight, adjustable compressive strength, good thermal insulation properties and easy production make it a widely used material in road embankments [1–6]. Cement, as the most dominant binder in foamed concrete, has an estimated energy consumption of approximately 7% of world total [7]. The process of calcination in cement production contributes 5% of the global CO_2 emissions [8,9]. With a vision of sustainable development, the cement industry is facing huge challenges in energy conservation and CO_2 emission reduction.

Alkali-activated slag (AAS) cement is known as an environment-friendly cementitious material which is produced by the reaction between ground granulated blast furnace slag and alkali activators [10,11]. In particular, the characteristics of high viscosity, self-compacting ability, and high strength of AAS cement are especially suitable for the preparation of lightweight foamed concrete [12]. Yang, Lee, et al. [13] used two types of alkali activators to activate GGBS and revealed that alkali activated GGBS developed higher compressive strength than OPC. Geopolymer and alkali-activated fly ash have also been used to replace OPC for producing foam concrete [14–16].

However, using strong alkalis, e.g. NaOH and $NaSiO_3$, as activators results in practical problems, such as rapid setting time, high cost, energy-intensive manufacturing and the risk of environmental contamination [17]. It has been verified that calcium hydroxide could be a practical and safe alternative to alkaline solutions. Its pH value is lower and setting time is longer than activators such as sodium hydroxide [18–26]. Since the production of hydrated lime is associated with high energy consumption and CO_2 emissions [27,28], Wen et al.[17] replaced hydrated lime with carbide slag (CS) to activate GGBS successfully, which results in both environmental and economic benefits. CS is a by-product of the hydrolysis of calcium carbide to generate acetylene, polyvinyl chloride and polyvinyl alcohol [29]. In China, the annual generation of CS in 2020 had increased to around 27.5 million tons [30]. Although CS has been used in CO_2 capture and cement production [31–33], the overall utilization rate is<10% [34]. CS is mainly composed of calcium hydroxide (>80%), which gives it great potential to produce foamed lightweight concrete for road embankments.

To ensure that the workability of the fresh slurry meets the in-situ construction requirements, the spreadability of the designed foamed concrete should be in the range of 160 and 190 mm according to the

* Corresponding authors.
E-mail addresses: zhige@sdu.edu.cn (Z. Ge), yfling@sdu.edu.cn (Y. Ling).

https://doi.org/10.1016/j.conbuildmat.2022.127840
Received 4 April 2022; Received in revised form 5 May 2022; Accepted 9 May 2022
Available online 30 May 2022

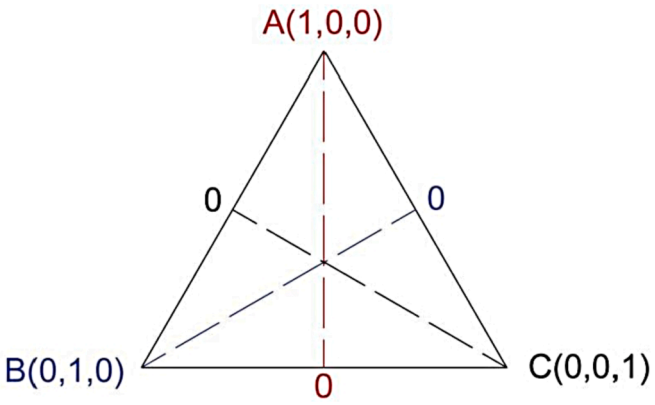

Fig. 1. Simplex Plot of Mixture Design.

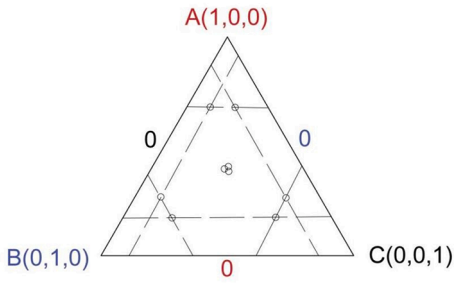

Fig. 2. Irregular mixture regions with possible relation constrains.

Table 1
Mixture constrains.

Low limit	Constraint	High limit
6.5	GGBS(V%)	20
0	CS/(CS + GGBS)(V%)	35
0.5	Water/slag(Mass ratio)	0.8
GGBS(V%) + CS(V%) + Water(V%) + Foam(V%) = 100%		

Chinese JTGD30-2015 standard. In terms of the foamed lightweight concrete made with cement, the spreadability can be controlled by adding additives like superplasticizers. However, for alkali activated materials, it is reported that the admixtures which improve workability may cause severe compressive strength decrease or activation delay [35]. Therefore, the control of alkali activated foamed concrete's spreadability could only be achieved by adjusting the volume ratio of all components. This makes the design process consumes huge amounts of labor power as well as material and financial resources. To simplify the try-and-error process, this study took the two key required properties of foam lightweight concrete, e.g. spreadability and compressive strength, as the target parameters. Through the statistical mixture design method, the regression models of spreadability and compressive strength were established. Finally, the derived numerical models were used to optimize the mixture that gives the optimum performance in terms of acceptable spreadability and high compressive strength.

2. Experimental design

Design of Experiment (DOE), as an efficient and accurate factor analysis method, has been applied in several areas such as analytical chemistry, food industry, paints and composites [36–38]. Recently, DOE has been adopted for construction material design, like ultra-high performance concrete (UHPC) [39], pervious concrete [40], bitumen formulations [41] and alkali-activated materials (AAMs) [42]. Compared with the one-factor-at-a-time experiments, DOE allows the investigation of how a factor affects a product or process in the presence of the others. Mixture design belongs to a typical group of DOE. It is assumed that the measured response value is only affected by the relative content and independent of absolute content of each ingredient [43]. The proportion of each component is between 0 and 1, the total amount must be 100%, and mixture factors cannot be manipulated completely independently of one another.

The factorial design, Taguchi design [44,45] has been applied in alkali activated materials. Different from these methods that use the Cartesian coordinate system, the experiment space of mixture design is limited to a simplex region, as shown in Fig. 1. When restrictions are introduced, the experiment area has to be reduced from the original simplex to an irregular polyhedron, as shown in Fig. 2 [46]. Therefore, an Extreme Vertex Design approach is required.

The mixture design method usually obeys the following steps: (1) define key properties for the product; (2) definite factors and constrains; (3) select an appropriate.

design algorithm; (4) execute design; (5) analyze data and evaluate model; (6) model confirmation; (7) optimization of product [41,46].

Four variables, namely GGBS, CS, water, and foam were involved. The total volume of the mixture was set as 1, where the content of each component was expressed in volume percent (V%). The percentage of GGBS was limited in a certain range, 6.5%-20%. As reported, an optimum CS/GGBS ratio for compressive strength development was 10% for 7 days and 5% for 28 days (mass ratio) [17]. In this study, the CS content was limited within 0%-35%, and the water to cement ratio constrain was set in a relatively large range to achieve a wide range of spreadability. The constraints of the mixture design used are shown in Table 1. Afterwards, 18 runs within the feasible region and boundaries were generated.

In order to simplify the mixing process of foamed lightweight concrete, the spreadability of fresh slurry and the compressive strengths at 3d, 7d and 28d age were taken as the target response. For the above irregular design space, the I-Optimal design method was applied [47]. It is suitable when the goal is to optimize one or more responses as it seeks to minimize the average prediction variance, and is often used to optimize the quadratic models. The Scheffe quadratic regression model, shown in Eq.(1), was used to simulate the response by combining the main effects (each of the individual component in the mixture) and two-factor interactions for each mixture component [48]:

$$E(Y) = \sum_{i=1}^{q} \beta_i x_i + \sum_{i=1}^{q-1} \sum_{j=i+1}^{q} \beta_{ij} x_i x_j \quad (1)$$

where $E(Y)$ is the expected value of the response y, q is the number of components, β_i is the expected response to pure component i, and β_{ij} is the expected change in response (from linear blending) due to the quadratic blending of components i and j [48].

3. Experimental procedure

3.1. Raw materials

The used local industrial solid wastes in the current study are S95 GGBS obtained from Heze Jingfu Granulated Furnace Slag Co., Ltd (Heze, Shandong Province) and CS obtained from Shandong Dongyue Chemical Co., Ltd (Zibo, Shandong). CS was dried in vacuum oven to a constant weight at 105℃ and then grounded. The density of GGBS and CS are 2900 kg/m^3 and 2185 kg/m^3 respectively. The particle size distribution of the grounded CS and GGBS are shown in Fig. 3. The specific surface area and median particle diameter of GGBS and CS are shown in Table 2. Clearly, after grinding, CS has a smaller particle size than GGBS. The chemical and Crystal compositions of the raw GGBS and CS were measured using X-ray fluorescence (XRF) and X-ray diffraction (XRD), respectively. The results are shown in Table 3 and Fig. 4. It can be seen

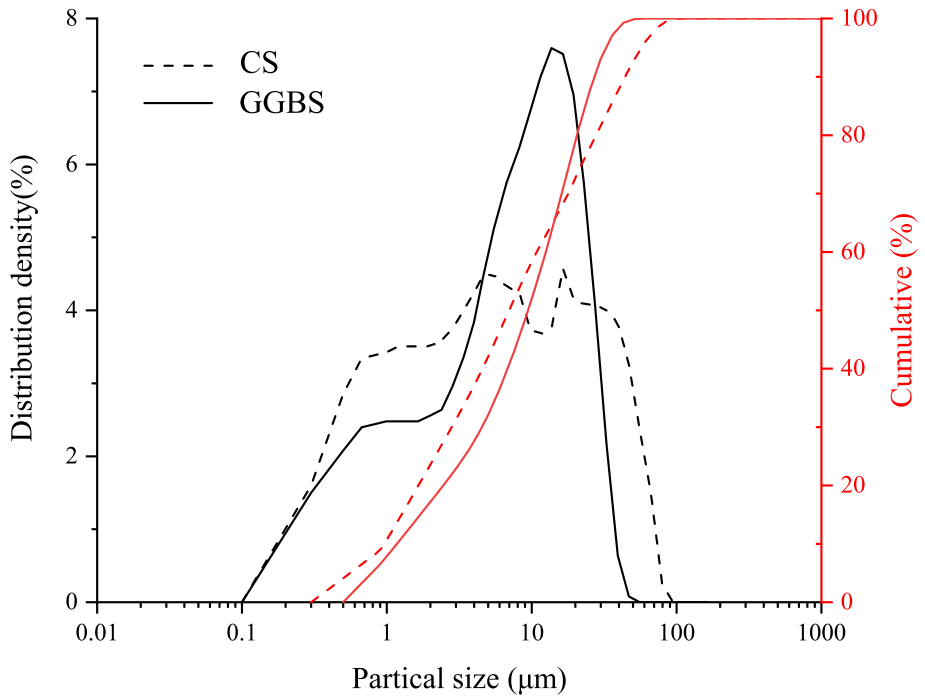

Fig. 3. Particle size distribution of CS, GGBS.

Table 2
Specific surface area (SSA) and median particle diameter (D_V50) of raw materials.

Material	GGBS	CS
SSA (m^2/g)	4.13	6.56
D_V50 (μm)	9.46	7.01

that CaO occupies 88.09% of CS by weight. As indicated by XRF, most of the calcium is in the form of $Ca(OH)_2$. No $CaCO_3$ was detected.

3.2. Preparation and characterization of foamed concrete

The foamed concrete was prepared by a pre-foaming method to avoid foam structure destruction during the stirring process. Firstly, CS was mixed with water, stirred at a low speed of 145 ± 5rm for 30 s. After that, GGBS was added and mixed at a low speed for 60 s. This was followed by another 60 s mixing under a speed of 285 ± 10rm. A protein-based anionic foaming agent purchased from Yantai Chilong Building Energy Saving Technology Co., LTD (Shandong, China) was used for configuring the foaming liquid. The used foaming agent-to-water ratio is 1/49. Compressed air was mixed with the foaming liquid in the foaming machine, and the density of the produced foam is 40 kg/m^3. Once the slurry was prepared, the weighed foam was added and mixed at a low speed of 145 ± 5rm until there was no white foam on the surface and the slurry was uniform.

Before casting the specimens, wet density and spreadability was measured. Wet density was calculated from the weight of mixture and the known volume of a standard vessel. The spreadability was measured using the Brewer test for controlled low-strength material [49]. This test only obtains the initial diffusion without vibration and slump flow, which is more suitable for construction sites. According to the provisions of the standard JTGD30-2015, the open-ended metal cylinder used to fill fresh mixture has a diameter of 108 mm and height of 109 mm. The spread in two directions were measured and the average value was used to represent the spreadability.

12 cubes with size of 100 mm were cast for each run. After pouring the fresh mixture into molds, the specimens were covered with plastic sheets and cured for 48 h under room temperature of 20 ± 1℃. The demolded specimens were then sealed by plastic bags and stored at 20 ± 1℃ until test. Compressive strength was measured following the Chinese GB/T 11969–2008 standard. For each mixture, three specimens were tested at 3d, 7d and 28d respectively. Note that some of the sample was too weak to be demolded until the test age. Their corresponding compressive strength was therefore regarded as 0.

4. Results and discussion

Table 4 presents the measured spreadability, 3d, 7d, and 28d compressive strengths of all the mixes. The spreadability varied from 123 mm to 235 mm, as we set a relatively large range in slag content and water to slag ratio. The 28d compressive strength ranges from 0 MPa to 5.2 MPa because some of the mixes do not get harden. As expected, the compressive strength increases with the curing age. Different from Portland cement concrete and AAS, the 28d compressive strength of the carbide residue activated blast furnace slag foamed lightweight concrete is two times higher than that in 7d.

4.1. Model of spreadability

Before a mix model was selected, the linear, quadratic, and special

Table 3
Chemical composition (%wt) of GGBS and CS.

Oxides	CaO	SiO_2	Al_2O_3	MgO	SO_3	Fe_2O_3	TiO_2	MnO	K_2O	Na_2O	Other
GGBS	39.06	31.83	14.70	8.72	2.83	0.40	1.03	0.52	0.38	0.31	0.22
CS	88.09	3.13	1.91	0.21	5.77	0.44	0.01	0.02	0.03	ND	0.39

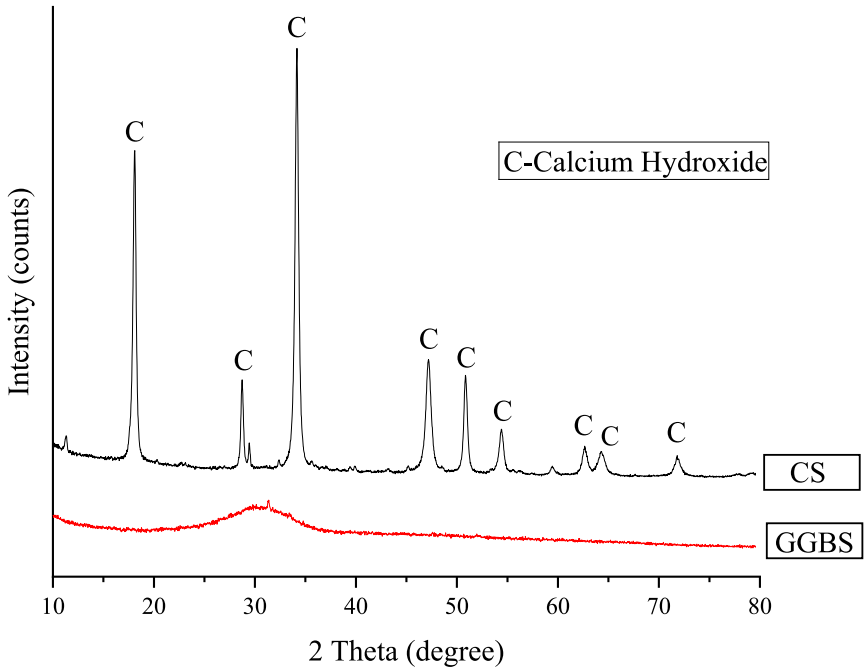

Fig. 4. X-ray diffraction of CS and GGBS.

Table 4
Set point combinations and corresponding experimental responses.

Run	GGBS(%)	CS(%)	H_2O(%)	Foam(%)	spread -ability(mm)	3d (MPa)	7d (MPa)	28d (MPa)
1	11.4	0.0	16.5	72.1	165	0.0	0.0	0.02
2	9.6	5.5	28.9	56.0	215	0.1	0.5	2.7
3	8.0	4.5	26.5	60.9	210	0.1	0.3	2.1
4	11.8	0.0	20.7	67.5	191	0.0	0.0	0.0
5	8.6	4.9	18.9	67.6	138	0.3	0.6	1.3
6	6.5	0.0	9.4	84.1	147	0.0	0.0	0.0
7	7.9	3.0	23.5	65.6	216	0.1	0.2	1.8
8	11.8	0.0	20.7	67.5	189	0.0	0.0	0.0
9	15.2	2.2	28.9	53.6	168	0.3	1.6	5.1
10	19.0	0.0	27.5	53.6	176	0.0	0.0	0.0
11	14.0	8.0	28.9	49.2	134	0.8	2.2	4.7
12	6.5	0.0	14.9	78.6	202	0.0	0.0	0.0
13	13.5	3.0	22.9	60.6	126	0.3	1.2	3.7
14	6.5	2.0	18.5	73.0	159	0.1	0.1	1.0
15	12.4	0.0	28.7	58.9	235	0.0	0.0	0.0
16	15.2	2.2	28.9	53.6	155	0.4	2.3	5.2
17	13.5	3.0	22.9	60.6	123	0.2	0.9	3.8
18	8.6	4.9	18.9	67.6	129	0.1	0.3	1.2

Table 5
ANOVA table for the model of spreadability.

Source	Sum of Squares	df	Mean Square	F-value	p-value	Significance
Model	19306.29	5	3861.26	29.82	< 0.0001	significant
Linear Mixture	16834.26	3	5611.42	43.34	< 0.0001	significant
GGBS*CS	1917.77	1	1917.77	14.81	0.0023	significant
CS*Foam	2445.16	1	2445.16	18.89	0.001	significant
Residual	1553.71	12	129.48			
Lack of Fit	1422.21	8	177.78	5.41	0.0603	not significant
Pure Error	131.5	4	32.88			
Cor Total	20,860	17				

Table 6
Analysis results for regression of the spreadability model.

Std. Dev.	Mean	C.V. %	R^2	Adjusted R^2	Predicted R^2	Adeq Precision
11.38	171.00	6.65	0.9255	0.8945	0.8464	16.0266

cubic models were calculated at first to provide reference for subsequent model selection. Statistics, such as p-value, lack of fit, and R^2 were used to detect the significance of these models. After that, a preferred Quadratic model given by Eq. (1) was used for regression of spreadability. The analysis of variance (ANOVA) table is a statistical test to assess whether or not any of the terms in the model contribute to explaining the response and the results of ANOVA were shown in Table 5. A small p-value (<0.0001) indicates that each of the main effects was significant at a confidence level of 95%. The two-factor interactions, GGBS*CS and CS*Foam, are both significant with p-value≪0.05, and other terms that p-value > 0.05 were eliminated to

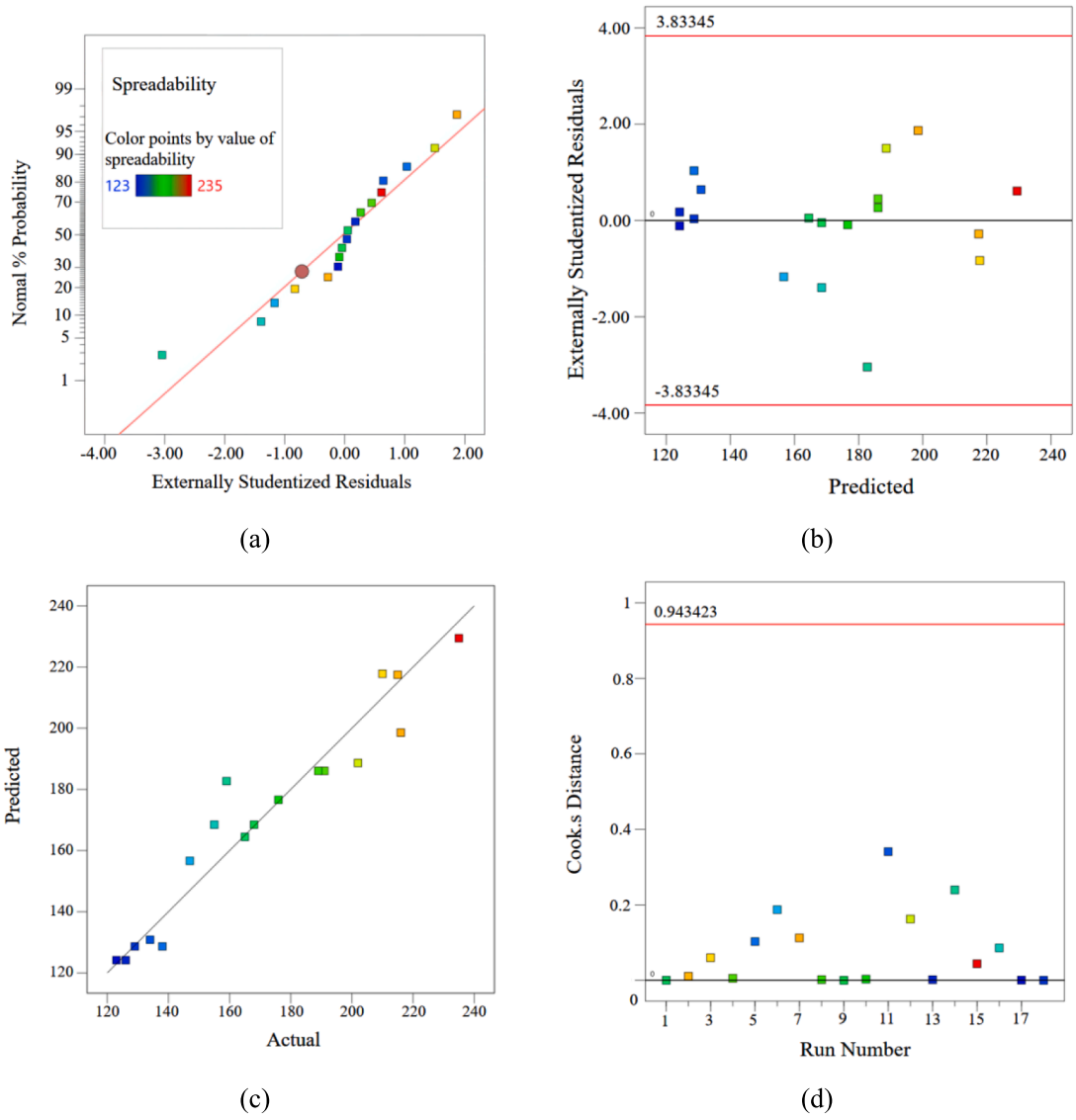

Fig. 5. Diagnostics analysis of spreadability model: (a)Normal Plot of Residuals, (b)Residual vs. Predicted, (c)Predicted vs. Actual, (d)Cook's Distance.

ensure the significance of the model. The lack of fit is found to be insignificant as the corresponding p-value is higher than 0.05. In addition to the ANOVA test, the adequacy of the proposed model was also validated by coefficients of multiple determination (R^2). As shown in Table 6, the R^2 of 0.9255 is in reasonable agreement with the R^2-adjusted of 0.8495 (the difference is<0.2). In general, R^2 values above 0.7 are considered fairly high. Adeq Precision measures the signal to noise; a ratio>4 is desirable. In this model, the Adeq Precision of 16.0266, corroborating the adequacy of the model used to navigate the design space. The final models obtained to predict spreadability is presented as Eq. (2).

$$\begin{aligned}\text{Spreadability (mm)} = &-5.47(\text{V\% GGBS}) + 75.72(\text{V\% CS}) \\ &+ 7.35(\text{V\% Water}) + 1.46(\text{V\% Foam}) \\ &- 2.72(\text{V\% GGBS})(\text{V\% CS}) \\ &- 0.97(\text{V\% CS})(\text{V\% Foam})\end{aligned} \tag{2}$$

The residuals are the differences between the responses observed at each combination values and the corresponding prediction of the response. If the model fit to the data were correct, the residuals would approximate the random errors that make the relationship between the explanatory variables and the response variable a statistical relationship. Therefore, if the residuals appear to behave randomly, it suggests that the model fits the data well. On the other hand, if non-random structure is evident in the residuals, it is a clear sign that the model fits the data poorly. To further verify the reliability of the model, a range of diagnostic tools like Normal Plot of Residuals (Fig. 5a), Residual vs. Predicted (Fig. 5b), Predicted vs. Actual (Fig. 5c) and Cook's Distance (Fig. 5d) were used. The normal probability plot is used to check whether it is reasonable to assume that the random residuals inherent in the process have been drawn from a normal distribution. The straight line indicates that the residuals follow a normal distribution, thus verifying that the residuals are random. The residual vs. Predicted plot compared the residuals and the ascending predicted response values and tested the assumption of constant variance. The linear distributed scatter in Fig. 5a and the random scatter in Fig. 5b indicates that the model fitted well without any transformation. The prediction performance of responses is detected by the Predicted vs. Actual plot as shown in Fig. 5c. It can be seen that predicted and experimental values are well correlated. Cook's Distance is a measure of the entire regression function when a specific run is not included for fitting the model. It is generally to identify possible outlier caused by experimental error or deviations from normal distribution and evaluate the influence during each run. As Fig. 5d shows, all runs are down below the red line, which means that there is no existence of outliers for the model.

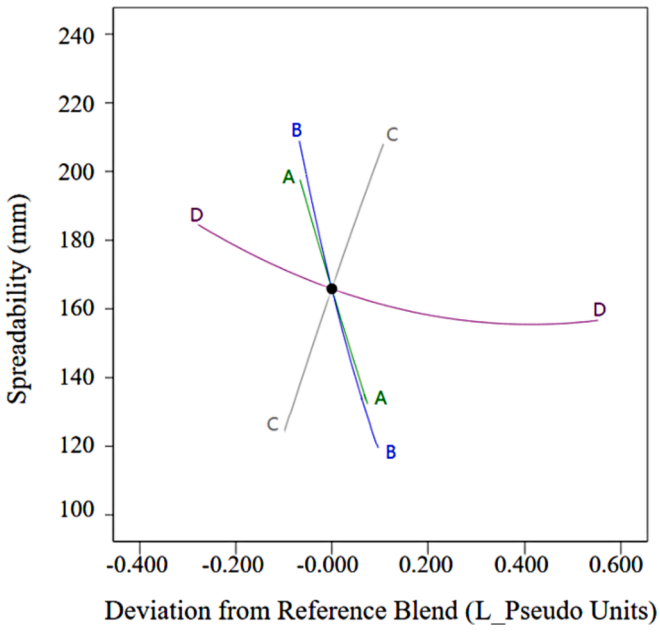

Fig. 6. Trace plot of the effect of component content on spreadability (A: GGBS; B: CS; C: Water; D: Foam).

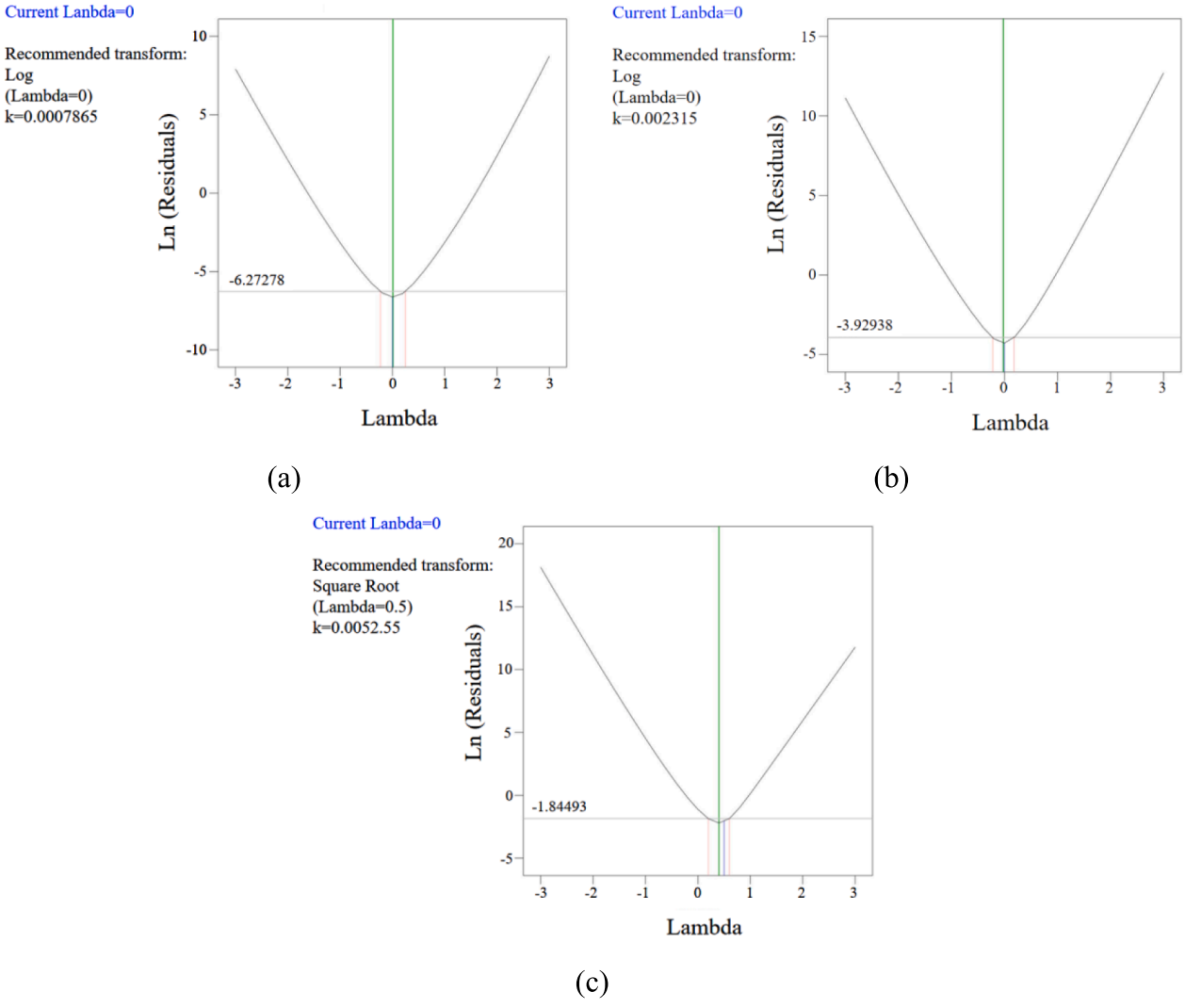

Fig. 7. Box-cox Plot for transformation analysis of compressive strength model: (a)3 days; (b)7 days; (c)28 days.

To have a better understanding on the effect of each individual component to the response, a trace plot (Fig. 6) displays the effect of parameter changes in the mixture on the predicted response. Obviously, the spreadability strongly depends on the GGBS, CS and water dosages. The content of solid wastes has significant negative effect, and water has a significant positive effect on the spreadability. In addition, the spreadability of the slurry decreased with the foam content. Similar trend has been reported in the previous studies on foamed concrete made with Portland cement [6,50].

4.2. Model of compressive strength

A transformation might be necessary when the residuals exhibit non-constant variance or non-normality. For example, if the response varies by more than a few orders of magnitude, a logarithmic transformation is usually adopted. It is well-known that the required response transformation highly relies on the form of response. The two non-power law, logit transformation for bounded data and arc sin-sqrt for proportions are the commonly used approaches [51]. The Box-cox plots for providing a guideline to select the correct power law transformation are presented in Fig. 7. The lowest point on the Box-cox plot represents the value of lambda (λ) that results in the minimum residual sum of squares in the transformed model. Based on this, a recommended transformation can be obtained. For the model of compressive strengths at different ages, the recommended transformations are shown as Fig. 7. They are logit (K = 0.0007865) for 3d compressive strength model, logit (K = 0.002315) for 7 days compressive strength model and square-root (K = 0.0052055) for 28 days compressive strength model, respectively. The transformed normal plots (Fig. 8) of residuals present an approximately linear trend which indicates that the residuals follow a normal distribution and no significant correlation existed between them.

On the basis of statistical analysis, the Quadratic model given by Eq. (1) was adopted for the regression of the compressive strength. ANOVA table of the compressive strength at 3 days, 7 days, and 28 days are shown in Table 7, Table 8 and Table 9, respectively. For all cases, the Linear mixture possesses a p-value < 0.0001, confirming that all main effects are significant. The two-factor interactions, GGBS*CS, CS*Water and CS*Foam are significant with p-value$\ll$0.05. Other terms whose p-value > 0.05 were eliminated from the model to guarantee the significance of the model. All the models reach the requirement of significance test and diagnostics analysis, as shown in Table 10. The adjusted-R^2 value of these models are 0.9662, 0.9715, 0.9850 respectively, which confirms the fitting adequacy. The compressive strength model at different ages is represented by Eq.(3), Eq.(4) and Eq.(5).

$$\begin{aligned}\ln(Y_3 + 0.0007865)(\text{MPa}) = &- 0.1495(\text{V\% GGBS}) - 22.8691(\text{V\% CS}) \\ &- 0.0254(\text{V\% Water}) - 0.0709(\text{V\% Foam}) \\ &+ 0.3727(\text{V\% GGBS})(\text{V\% CS}) \\ &+ 0.2231(\text{V\% CS})(\text{V\% Water}) \\ &+ 0.2431(\text{V\% CS})(\text{V\% Foam})\end{aligned} \tag{3}$$

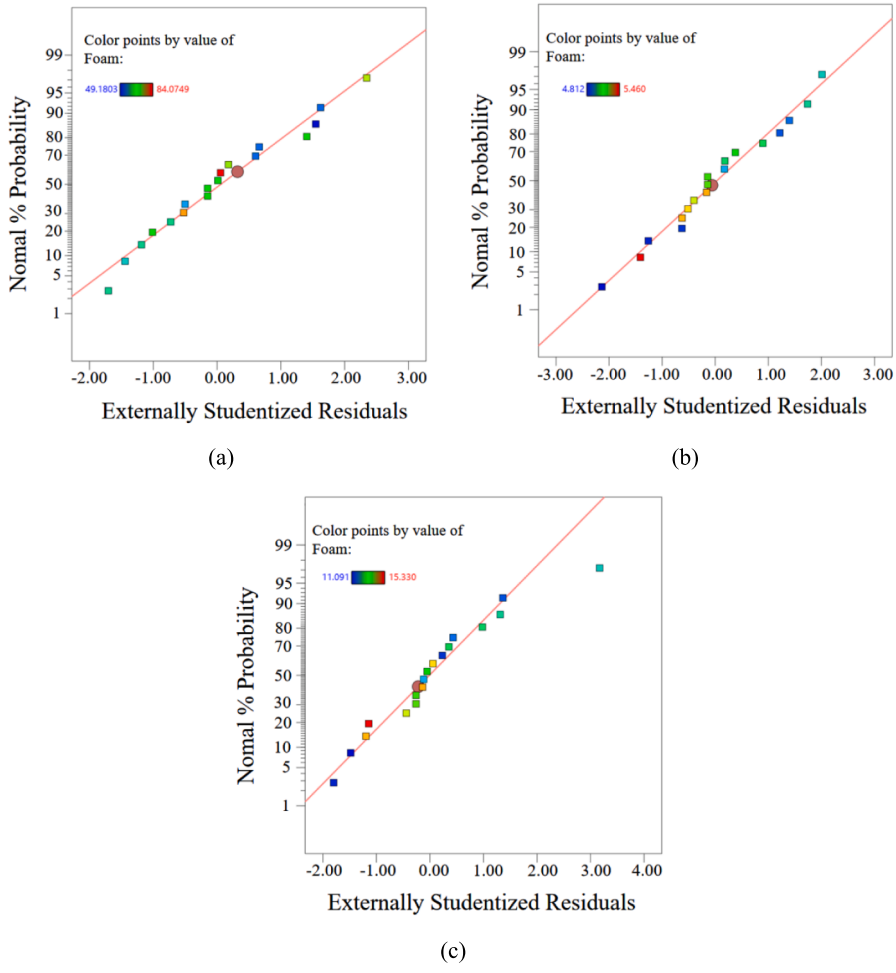

Fig. 8. Residual normal plot of compressive strength model: (a)3 days; (b)7 days; (c)28 days.

Table 7
ANOVA table for the 3 d compressive strength.

Source	Sum of Squares	df	Mean Square	F-value	p-value	Significance
Model	128.95	6	21.49	28.05	< 0.0001	significant
Linear Mixture	97.21	3	32.40	123.72	< 0.0001	significant
GGBS*CS	26.07	1	26.07	99.52	< 0.0001	significant
CS*Water	9.30	1	9.30	35.52	< 0.0001	significant
CS*Foam	20.89	1	20.89	79.78	< 0.0001	significant
Residual	2.88	11	0.2619			
Lack of Fit	2.39	7	0.3410	2.76	0.1718	not significant
Pure Error	0.4944	4	0.1236			
Cor Total	131.83	17				

Table 8
ANOVA table for the 7 d compressive strength.

Source	Sum of Squares	df	Mean Square	F-value	p-value	Significance
Model	142.02	6	23.67	97.64	< 0.0001	significant
Linear Mixture	100.16	3	33.39	137.72	< 0.0001	significant
GGBS*CS	35.78	1	35.78	147.58	< 0.0001	significant
CS*Water	15.22	1	15.22	62.77	< 0.0001	significant
CS*Foam	30.33	1	30.33	125.10	< 0.0001	significant
Residual	2.67	11	0.2424			
Lack of Fit	2.29	7	0.3278	3.52	0.1205	not significant
Pure Error	0.3722	4	0.0931			
Cor Total	144.69	17				

$$\ln(Y_7 + 0.002315)(\text{MPa}) = -0.1263(\text{V\% GGBS}) - 28.0017(\text{V\% CS}) - 0.018605(\text{V\% Water}) - 0.0610(\text{V\% Foam}) + 0.4366(\text{V\% GGBS})(\text{V\% CS}) + 0.2853(\text{V\% CS})(\text{V\% Water}) + 0.2929(\text{V\% CS})(\text{V\% Foam}) \quad (4)$$

$$\sqrt{Y_{28} + 0.005206}(\text{MPa}) = -0.0077(\text{V\% GGBS}) - 9.7397(\text{V\% CS}) - 0.0064(\text{V\% Water}) - 0.0008(\text{V\% Foam}) + 0.1460(\text{V\% GGBS})(\text{V\% CS}) + 0.1079(\text{V\% CS})(\text{V\% Water}) + 0.0983(\text{V\% CS})(\text{V\% Foam}) \quad (5)$$

Fig. 9 shows the trace plot for 28d compressive strength. It represents the effect of component variation on compressive strength, and the slope of the graph indicates the sensitivity of the response to each component. As it can be seen, foam content has a major influence on the compressive strength. This is expected, as foam content dominates the density of the hardened material. It is found that compressive strength decreases significantly with the density. In the previous studies, the dry density varies from 280 to 1800 kg/m^3 by which the compressive strength at 28 days increased from 0.6 MPa to 43 MPa[52,53]. The water content also

Table 10
Analysis results for regression of the compressive strength model.

Responses	Adj-R^2	Pre-R^2
3d compressive strength	0.9662	0.8645
7d compressive strength	0.9715	0.9092
28d compressive strength	0.9850	0.9490

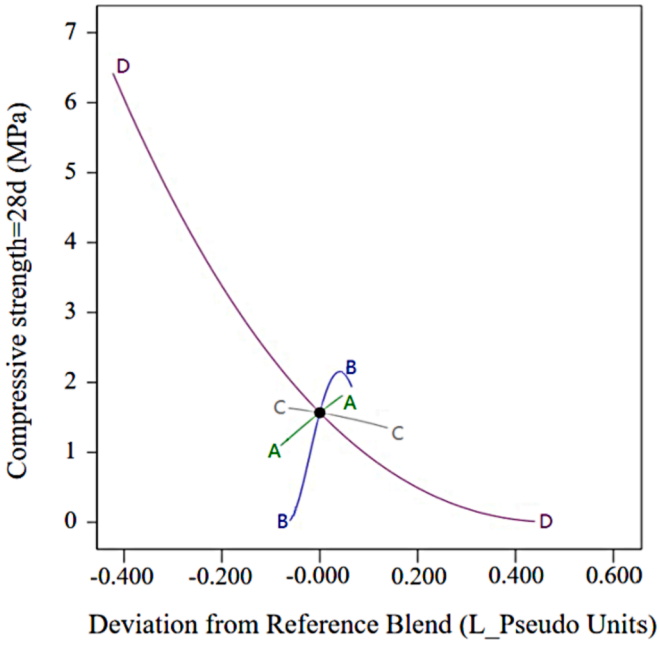

Fig. 9. Trace plot of the effect of component content on compressive strength (A: GGBS; B: CS; C: Water; D: Foam).

Table 11
Run ingredients for model confirmation.

Run	GGBS(V%)	CS(V%)	Water(V%)	Foam(V%)
1	7.87	3.11	23.54	65.48
2	12.72	1.88	26.65	58.75

Table 9
ANOVA table for the 28 d compressive strength.

Source	Sum of Squares	df	Mean Square	F-value	p-value	Significance
Model	12.44	6	2.07	187.65	< 0.0001	significant
Linear Mixture	8.16	3	2.72	246.04	< 0.0001	significant
GGBS*CS	4.00	1	4.00	362.24	< 0.0001	significant
CS*Water	2.17	1	2.17	196.85	< 0.0001	significant
CS*Foam	3.42	1	3.42	309.18	< 0.0001	significant
Residual	0.1215	11	0.0110			
Lack of Fit	0.1057	7	0.0151	3.81	0.1070	not significant
Pure Error	0.0159	4	0.0040			
Cor Total	12.56	17				

Table 12
Comparison between predicted and experimental results.

	run 1				run 2			
	Experi-mental	Predi-cted	95% PI low	95% PI high	Experi-mental	Predi-cted	95% PI low	95% PI high
spreadability	216	198	171	225	170	182	156	209
3d compressive strength	0.07	0.09	0.02	0.26	0.17	0.07	0.02	0.20
7d compressive strength	0.24	0.31	0.08	0.90	0.58	0.32	0.09	0.92
28d compressive strength	1.76	1.82	1.19	2.56	3.11	2.47	1.73	3.30

Table 13
Settings for mixture optimization with maximized 28 d compressive strength.

Parameter	Lower limit	Upper limit	Goal
GGBS	6.5	19.9	in range
CS	0	7.9	in range
Water	9.1	28.9	in range
Foam	49.2	84.1	in range
Spreadability	160	190	in range
28 d Compressive strength	0	–	maximize

Table 15
Settings for mixture optimization with maximized CS content.

Parameter	Lower limit	Upper limit	Goal
GGBS	6.5	19.9	in range
CS	0	7.9	maximize
Water	9.1	28.9	in range
Foam	49.2	84.1	in range
Spreadability	160	190	in range
7d compressive strength	0.4	–	in range
28d compressive strength	0.8	–	in range

has a remarkable influence on the compressive strength, but not as much as the foam. GGBS as a main resource of hydration products has a significant contribution to compressive strength. CS is the activator of GGBS. However, the compressive strength does not always increase with the CS. This can be explained as that when the relative content of CS reaches a specific value, a further increase of CS leads to a subsequent reduction of precursor amount[17].

4.3. Model validation

To verify the accuracy of the model, two mixtures within the constrains (see Table 1) were generated. The ingredients in each of the confirmation runs are presented in Table 11. The measured spreadability and compressive strengths are compared with the predictions in Table 12 It shows that all confirmation runs fall within the 95% prediction interval of the model, confirming that the proposed model (Eq.2–5) is capable to predict the spreadability and compressive strength of carbide residue activated blast furnace slag foamed lightweight concrete within the mixture constrains.

4.4. Mixture optimization

After validation, this model was further used to optimize the mixture. In the process of numerical optimization, several response variables were transformed into a desirability function and optimized by univariate analysis. The optimal solutions tend to satisfy the requirements of each response as much as possible without unduly compromising any requirements [54].

To realize an optimized combination of fluctuant components, the desired goal for each factor and response is chosen according to the requirements of the experimenter. For both factors and responses, meaningful goals could be set as “In range” (specify a range for acceptable results), “Maximize” (maximize the value of specified factors or responses), “Minimize” (minimize the value of specified factors or responses), and “Target” (set an optimal expected value satisfying factor constraints). In this study, a feasible mix is required to satisfy both workability and mechanical properties that refer to spreadability and compressive strength. According to standard JTGD30-2015, the target range of spreadability was set as 160 mm-190 mm and the desired response of compressive strength was defined as maximum.

To quantize the desirability of optimization, a multiple response method proposed by Myers et al.[55] was adopted. It applies an objective function $D(X)$ and is termed as desirability function:

$$D = (d_1 \cdot d_2 \cdot \ldots \cdot d_n)^{\frac{1}{n}} = \left(\prod_{i=1}^{n} d_i\right)^{\frac{1}{n}} \tag{6}$$

where n is the number of responses included in the measure. Individual desirability function (d_i) range between 0, for fully undesired response, and 1, for totally desired response. For values of D close to 1, the combination of different criteria is globally optimal, so the response value is also close to the target value. If any responses or factors fall outside their desirability range, the overall function becomes zero.

For simultaneous optimization, each factor or response should be included in the optimization range by default, or as a maximum, minimum of target value. For the two constraints imposed on the above-mentioned spreadability and compressive strength, the desirability of “In range” and “Maximum” can be defined by Eq.(7) and (8), respectively:

$$d = \begin{cases} 0 & Y_i \le L \\ 1 & L < Y_i < H \\ 0 & Y_i \ge H \end{cases} \tag{7}$$

$$\begin{cases} d_i = 0 & Y_i < L \\ 0 < d_i < 1 & L < Y_i < H \\ d_i = 1 & Y_i > H \end{cases} \tag{8}$$

where L represents the low value of defined parameter interval, and H represents the high value of defined parameter interval. The maximum and minimum limits of all factors and responses are listed in Table 13. Table 14 shows five optimal solutions at the end of the multi-objective optimization process. The desirability of all designed mixes

Table 14
Optimized solutions for mix with maximized compressive strength.

number	GGBS	CS	Water	Foam	Spreadability	3d	7d	28d	Desirability
1	12.8	5.3	28.6	53.3	163	1.02	6.44	6.67	1
2	12.7	4.7	28.7	54.0	173	0.66	4.00	5.88	1
3	12.6	6.0	28.9	52.5	165	1.01	4.50	5.76	1
4	14.1	3.6	28.9	53.4	172	0.97	4.66	5.62	1
5	11.6	4.8	28.5	55.0	183	0.67	3.33	5.27	1

Table 16
Optimized solutions for mixtures with maximized CS.

number	GGBS	CS	Water	Foam	Spreadability	3d	7d	28d	Desirability
1	12.7	7.2	28.9	51.2	160	0.49	1.58	4.12	0.905
2	11.7	6.7	27.4	54.1	160	0.42	1.27	3.42	0.841
3	10.8	6.2	28.4	54.6	190	0.28	0.97	3.37	0.775
4	9.2	5.3	25.9	59.6	190	0.19	0.59	2.34	0.662
5	8.9	5.1	22.5	63.6	160	0.19	0.51	1.72	0.636

reaches 1 and the optimal 28 d compressive strength is 6.67 MPa.

Another optimization was made on design foamed concrete embankment with large CS content, as it can offer a way of mass consumption of CS. According to the specification of the Chinese JTG D30-2015 standard for the in-situ foamed lightweight concrete embankment, the compressive strength of the cast-in-place material should be no<0.4 MPa at 7 days and 0.8 MPa at 28 days. Minimum limits were imposed on 7d compressive strength as 0.4 MPa and 28d strength as 0.8 MPa. Maximization of CS content was added. Table 15 shows all limits of the factors and responses. The optimized results are shown in Table 16. As it can be seen that the maximum CS content that can be used to produce the foamed lightweight concrete embankment is 7.2%.

5. Conclusions

This paper has shown that it is possible to produce foamed lightweight concrete made of GGBS and CS that have acceptable spreadability and compressive strength required by the cast-in-situ road embankment construction. The main conclusions are as follows:

- All main effects are significant in each of the models. In terms of the the two-factor interactions, GGBS*CS and CS*Foam are significant in the spreadability regression model. GGBS*CS, CS*Water and CS*Foam are significant in the compressive strength models.
- The experimental responses, namely spreadability and 3d, 7d, 28d compressive strength, were successfully fitted to Scheffe quadratic models. The high value of adjusted-R^2 and diagnose analysis confirm the adequacy of the proposed models.
- Trace plots reveal that the spreadability strongly depends on the GGBS, CS and water dosages, and the compressive strength is mainly affected by the foam content.
- With acceptable spreadability, the optimized mixture can have a 28d compressive strength as high as 6.67 MPa. The maximum CS content that can be used to produce the foamed lightweight concrete embankment is 7.2%.

CRediT authorship contribution statement

Hongzhi Zhang: Methodology, Supervision, Writing – review & editing. **Yanchen He:** Investigation, Writing – original draft. **Yanhua Guan:** Funding acquisition, Methodology, Supervision, Writing – review & editing. **Chuan Wang:** Funding acquisition, Methodology. **Zhi Ge:** Writing – review & editing. **Renjuan Sun:** Writing – review & editing. **Yifeng Ling:** Funding acquisition, Methodology, Supervision, Writing – review & editing. **Branko Šavija:** Writing – review & editing.

Declaration of Competing Interest

The authors declare that they have no known competing financial interests or personal relationships that could have appeared to influence the work reported in this paper.

Acknowledgments

This work was supported by the National Natural Science Foundation of China (No. 52008234, 51478252, 51978387), Taishan Scholars Foundation of Shandong Province (No. tsqn201909032), Natural Science Foundation of Jiangsu Province (No. BK20200235) and Natural Science Foundation of Shandong Province (No. ZR2021QE174).

References

[1] M. Jones, A. McCarthy, Utilising unprocessed low-lime coal fly ash in foamed concrete, Fuel 84 (11) (2005) 1398–1409.
[2] P.J. Tikalsky, J. Pospisil, W. MacDonald, A method for assessment of the freeze–thaw resistance of preformed foam cellular concrete, Cement and concrete research 34 (5) (2004) 889–893.
[3] A. Giannakou, M. Jones, in: Potential of foamed concrete to enhance the thermal performance of low-rise dwellings, Thomas Telford Publishing, 2002, pp. 533–544.
[4] Z. Li, H. Yuan, F. Gao, H. Zhang, Z. Ge, K. Wang, R. Sun, Y. Guan, Y. Ling, N. Jiang, A Feasibility Study of Low Cement Content Foamed Concrete Using High Volume of Waste Lime Mud and Fly Ash for Road Embankment, Materials 15 (1) (2021) 86.
[5] H. Yuan, Z. Ge, R. Sun, X. Xu, Y. Lu, Y. Ling, H. Zhang, Drying shrinkage, durability and microstructure of foamed concrete containing high volume lime mud-fly ash, Construction and Building Materials 327 (2022), 126990.
[6] Z. Ge, H. Yuan, R. Sun, H. Zhang, W. Wang, H. Qi, Use of green calcium sulphoaluminate cement to prepare foamed concrete for road embankment: A feasibility study, Construction and Building Materials 237 (2020) 117791.
[7] I. Maruyama, W. Kotaka, B.N. Kien, R. Kurihara, M. Kanematsu, H. Hyodo, H. Hirao, R. Kitagaki, M. Tamura, M. Tsujino, A New Concept of Calcium Carbonate Concrete using Demolished Concrete and CO2, Journal of Advanced Concrete Technology 19 (10) (2021) 1052–1060.
[8] N. Chatziaras, C. Psomopoulos, N. Themelis, Use of alternative fuels in cement industry, in: Proceedings of the 12th International Conference on Protection and Restoration of the Environment, 2014, pp. 521–529.
[9] E. Gartner, H. Hirao, A review of alternative approaches to the reduction of CO2 emissions associated with the manufacture of the binder phase in concrete, Cement and Concrete Research 78 (2015) 126–142.
[10] T. Luukkonen, Z. Abdollahnejad, J. Yliniemi, P. Kinnunen, M. Illikainen, One-part alkali-activated materials: A review, Cement and Concrete Research 103 (2018) 21–34.
[11] A. Hassan, M. Arif, M. Shariq, Use of geopolymer concrete for a cleaner and sustainable environment – A review of mechanical properties and microstructure, Journal of Cleaner Production 223 (2019) 704–728.
[12] J. He, Q. Gao, X. Song, X. Bu, J. He, Effect of foaming agent on physical and mechanical properties of alkali-activated slag foamed concrete, Construction and Building Materials 226 (2019) 280–287.
[13] K.-H. Yang, K.-H. Lee, J.-K. Song, M.-H. Gong, Properties and sustainability of alkali-activated slag foamed concrete, Journal of Cleaner Production 68 (2014) 226–233.
[14] K. Ramamurthy, E.K. Kunhanandan Nambiar, G. Indu Siva Ranjani, A classification of studies on properties of foam concrete, Cement and Concrete Composites 31(6) (2009) 388-396.
[15] P. Hlaváček, V. Šmilauer, F. Škvára, L. Kopecký, R. Šulc, Inorganic foams made from alkali-activated fly ash: Mechanical, chemical and physical properties, Journal of the European Ceramic Society 35 (2) (2015) 703–709.
[16] S. Zhuang, Q. Wang, Inhibition mechanisms of steel slag on the early-age hydration of cement, Cement and Concrete Research 140 (2021), 106283.
[17] W. Li, Y. Yi, Use of carbide slag from acetylene industry for activation of ground granulated blast-furnace slag, Construction and Building Materials 238 (2020) 117713.
[18] C. Shi, D. Roy, P. Krivenko, Alkali-activated cements and concretes, CRC press2003.
[19] F. Bellmann, J. Stark, Activation of blast furnace slag by a new method, Cement and Concrete Research 39 (8) (2009) 644–650.
[20] Y. Jeong, J.E. Oh, Y. Jun, J. Park, J.-H. Ha, S.G. Sohn, Influence of four additional activators on hydrated-lime [Ca(OH) 2] activated ground granulated blast-furnace slag, Cement and Concrete Composites 65 (2016) 1–10.
[21] Y. Jeong, H. Park, Y. Jun, J.H. Jeong, J.E. Oh, Influence of slag characteristics on strength development and reaction products in a CaO-activated slag system, Cement and Concrete Composites 72 (2016) 155–167.
[22] M.S. Kim, Y. Jun, C. Lee, J.E. Oh, Use of CaO as an activator for producing a price-competitive non-cement structural binder using ground granulated blast furnace slag, Cement and Concrete Research 54 (2013) 208–214.
[23] J. Lei, W.W. Law, E.-H. Yang, Effect of calcium hydroxide on the alkali-silica reaction of alkali-activated slag mortars activated by sodium hydroxide, Construction and Building Materials 272 (2021) 121868.

[24] J. Wang, X. Lyu, L. Wang, X. Cao, Q. Liu, H. Zang, Influence of the combination of calcium oxide and sodium carbonate on the hydration reactivity of alkali-activated slag binders, Journal of Cleaner Production 171 (2018) 622–629.
[25] D. Wang, Q. Wang, Z. Huang, New insights into the early reaction of NaOH-activated slag in the presence of CaSO4, Composites Part B: Engineering 198 (2020) 108207.
[26] H. Bilal, T. Chen, M. Ren, X. Gao, A. Su, Influence of silica fume, metakaolin & SBR latex on strength and durability performance of pervious concrete, Construction and Building Materials 275 (2021).
[27] P.A.O. George, A.S. Gutiérrez, J.B.C. Martínez, C. Vandecasteele, Cleaner production in a small lime factory by means of process control, Journal of cleaner production 18 (12) (2010) 1171–1176.
[28] A.S. Gutiérrez, J. Van Caneghem, J.B.C. Martínez, C. Vandecasteele, Evaluation of the environmental performance of lime production in Cuba, Journal of Cleaner Production 31 (2012) 126–136.
[29] Y. Li, H. Liu, R. Sun, S. Wu, C. Lu, Thermal analysis of cyclic carbonation behavior of CaO derived from carbide slag at high temperature, Journal of Thermal Analysis and Calorimetry 110 (2) (2011) 685–694.
[30] X. Gong, T. Zhang, J. Zhang, Z. Wang, J. Liu, J. Cao, C. Wang, Recycling and utilization of calcium carbide slag - current status and new opportunities, Renewable and Sustainable Energy Reviews 159 (2022) 112133.
[31] X. Gao, X. Yao, T. Yang, S. Zhou, H. Wei, Z. Zhang, Calcium carbide residue as auxiliary activator for one-part sodium carbonate-activated slag cements: compressive strength, phase assemblage and environmental benefits, Construction and Building Materials 308 (2021).
[32] S. Dueramae, W. Tangchirapat, P. Sukontasukkul, P. Chindaprasirt, C. Jaturapitakkul, Investigation of compressive strength and microstructures of activated cement free binder from fly ash - calcium carbide residue mixture, Journal of Materials Research and Technology 8 (5) (2019) 4757–4765.
[33] T. Phoo-ngernkham, C. Phiangphimai, D. Intarabut, S. Hanjitsuwan, N. Damrongwiriyanupap, L.-Y. Li, P. Chindaprasirt, Low cost and sustainable repair material made from alkali-activated high-calcium fly ash with calcium carbide residue, Construction and Building Materials 247 (2020) 118543.
[34] M. Jiang, X. Huang, H. Liu, F. Zhan, Y. He, B. Li, Research progress on resource utilization of carbide slag, Bulletin of the Chinese Ceramic society 35 (12) (2016) 4025–4031.
[35] A.M. Rashad, A comprehensive overview about the influence of different additives on the properties of alkali-activated slag – A guide for Civil Engineer, Construction and Building Materials 47 (2013) 29–55.
[36] M.A. Bezerra, V.A. Lemos, C.G. Novaes, R.M. de Jesus, H.R. Souza Filho, S. A. Araújo, J.P.S. Alves, Application of mixture design in analytical chemistry, Microchemical Journal 152 (2020), 104336.
[37] M.F. Khan, D. Dwivedi, S. Sharma, Development of response surface model for tensile shear strength of weld-bonds of aluminium alloy 6061 T651, Materials & Design 34 (2012) 673–678.
[38] M. Tayefi, M. Razavi-Nouri, A. Sabet, Using constrained mixture design method for optimizing the properties of organoclay filled ethylene-octene copolymer nanocomposites, Materials Research Express 7 (1) (2020) 015321.
[39] E. Ghafari, H. Costa, E. Júlio, Statistical mixture design approach for eco-efficient UHPC, Cement and Concrete Composites 55 (2015) 17–25.
[40] A. Joshaghani, A.A. Ramezanianpour, O. Ataei, A. Golroo, Optimizing pervious concrete pavement mixture design by using the Taguchi method, Construction and Building Materials 101 (2015) 317–325.
[41] C. Varanda, I. Portugal, J. Ribeiro, A.M.S. Silva, C.M. Silva, Optimization of bitumen formulations using mixture design of experiments (MDOE), Construction and Building Materials 156 (2017) 611–620.
[42] K. Ellis, R. Silvestrini, B. Varela, N. Alharbi, R. Hailstone, Modeling setting time and compressive strength in sodium carbonate activated blast furnace slag mortars using statistical mixture design, Cement and Concrete Composites 74 (2016) 1–6.
[43] D.C. Montgomery, Design and analysis of experiments, John wiley & sons2017.
[44] A. Nazari, J.G. Sanjayan, Hybrid effects of alumina and silica nanoparticles on water absorption of geopolymers: Application of Taguchi approach, Measurement 60 (2015) 240–246.
[45] F. Puertas, S. Martínez-Ramírez, S. Alonso, T. Vázquez, Alkali-activated fly ash/slag cements: strength behaviour and hydration products, Cement and concrete research 30(10) (2000) 1625-1632.
[46] L. Eriksson, E. Johansson, C. Wikström, Mixture design—design generation, PLS analysis, and model usage, Chemometrics and Intelligent Laboratory Systems 43 (1–2) (1998) 1–24.
[47] U. Syafitri, B. Sartono, P. Goos, I-Optimal Design of Mixture Experiments in the Presence of Ingredient Availability Constraints, Journal of Quality Technology 47 (3) (2017) 220–234.
[48] G.F. Piepel, J.M. Szychowski, J.L. Loeppky, Augmenting Scheffé Linear Mixture Models with Squared and/or Crossproduct Terms, Journal of Quality Technology 34 (3) (2018) 297–314.
[49] W.E. Brewer, Controlled low strength materials (CLSM), Concrete in the Service of Mankind, CRC Press (1996) 664–675.
[50] E. Kunhanandan Nambiar, K. Ramamurthy, Fresh state characteristics of foam concrete, J. Mater. Civ. Eng. 20 (2) (2008) 111–117.
[51] D.M. Miller, Reducing transformation bias in curve fitting, The American Statistician 38 (2) (1984) 124–126.
[52] Y.H.M. Amran, N. Farzadnia, A.A. Abang Ali, Properties and applications of foamed concrete; a review, Construction and Building Materials 101 (2015) 990–1005.
[53] K. Ramamurthy, E.K. Nambiar, G.I.S. Ranjani, A classification of studies on properties of foam concrete, Cement and concrete composites 31 (6) (2009) 388–396.
[54] G. Derringer, R. Suich, Simultaneous optimization of several response variables, Journal of quality technology 12 (4) (1980) 214–219.
[55] R.H. Myers, A.I. Khuri, W.H. Carter, Response surface methodology: 1966–l988, Technometrics 31 (2) (1989) 137–157.